Impact of the distribution pattern of fast polarization scrambler on the performance of PMD mitigation with FEC for DQPSK optical system

Dahai Han (韩大海)*, Lixia Xi (席丽霞), Minliang Li (李敏良), Haoran Chen (陈浩然), and Feifei Liu (刘菲菲)

Key Laboratory of Information Photonics and Optical Communications (Beijing University of Posts and Telecommunications), Ministry of Education, Beijing 100876, China

**Corresponding author: dahaihan@gmail.com*

Received December 31, 2010; accepted April 11, 2011; posted online June 16, 2011

The combination of fast polarization scrambler (FPS) and forward error correction (FEC) is one of the methods to mitigate the polarization mode dispersion (PMD) in high-speed optical fiber communication systems. The effect of the different distribution patterns of FPS on PMD mitigation with FEC is investigated. A comparison of the bit error rates (BERs) between two cases where the distributed FPS is absent and present along the fiber is carried out by simulation. A novel representation called the "ring chart" to assess the performance of different distribution patterns intuitively is proposed. The results show that the distribution pattern is an impact factor for this PMD mitigation scheme.

OCIS codes: 060.0060, 230.0230, 250.0250.

doi: 10.3788/COL201109.070604.

The contradiction between the increase in optical transmission rate and the deterioration of the signal caused by polarization mode dispersion (PMD) has become more apparent in recent years. To address this challenge, researchers focused on the study of PMD compensation and mitigation techniques[1,2]. The combination of forward error correction (FEC) and distributed fast polarization scramblers (D-FPSs) as one of the PMD mitigation schemes has been proposed and presents a remarkable effect[3,4]. Compared with general PMD compensation schemes, this combination scheme shows the advantage of all-channels simultaneous mitigation and requirement for less time owing to the absence of feedback control[5]. Optical system margin can be expanded when FEC codes are regarded as a portion of it, while PMD tolerance for a given PMD penalty cannot be enlarged as the number of errors induced by PMD is beyond the error correction ability of the FEC[6]. PMD tolerance can be increased to a certain extent when the FPS is used in conjunction with FEC[4,7].

The differential group delay (DGD) is changing over the fiber link because of the stochastic feature of PMD; therefore, the FPS distribution pattern demonstrated in previous studies, which is typically uniform distribution, also has effect on the PMD mitigation performance. In this letter, various distribution patterns of FPS for differential quadrature phase-shift-keying (DQPSK) system are investigated, and a novel representation is used to clarify this effect.

The role of FPS in the fiber link is to accelerate the convergence of DGD's probability density function to Maxwellian distribution, instead of decreasing the numeric value of PMD, thus PMD-induced consecutive errors whose length exceeds the burst error correctable length (BECL) of FEC can be inhibited effectively[5,8]. In our simulation, a structure of $\lambda/4$, $\lambda/2$, and $\lambda/4$ wave plates cascaded sequentially comprises the FPS, whose three cells are all angle-adjustable and retardation-fixed plates[9]. The Jones matrices of this FPS can be denoted as

$$\begin{aligned}\mathbf{U_p} &= \mathbf{M}(\lambda/4)\cdot\mathbf{M}(\lambda/2)\cdot\mathbf{M}(\lambda/4)\\ &= -\cos\alpha\cdot\cos\beta\cdot\sigma_0 + \mathrm{i}\cdot\sin\alpha\cdot\cos\beta\cdot\sigma_2\\ &\quad -\mathrm{i}\cdot\sin\beta\cdot\sin\gamma\cdot\sigma_3 - \mathrm{i}\cdot\sin\beta\cdot\cos\gamma\cdot\sigma_1, \end{aligned} \quad (1)$$

where $\mathbf{M}(\lambda/4)$ and $\mathbf{M}(\lambda/2)$ are the Jones matrices of the quarter wave plate and the half wave plate, respectively; σ_i (i = 0,1,2,3) is the Pauli spin matrices, as defined in Ref. [10]; α, β, and γ are donated as

$$\alpha = \theta_1 - \theta_3, \quad \beta = 2\theta_2 - (\theta_1 + \theta_3), \quad \gamma = \theta_1 + \theta_3, \quad (2)$$

where θ_1, θ_2, and θ_3 are the azimuths of three wave plates, respectively. Each azimuth varies sinusoidally, and there is a slight distinction between each two frequencies of the drive voltages so the FPS can scramble over the entire Poincaré sphere.

$$\theta_1 = \frac{\pi}{2}\sin(2\pi f\cdot t), \quad (3a)$$

$$\theta_2 = \frac{\pi}{2}\sin[2\pi(f+\Delta f)\cdot t], \quad (3b)$$

$$\theta_3 = \frac{\pi}{2}\sin[2\pi(f+2\Delta f)\cdot t], \quad (3c)$$

where f is the fundamental frequency for the three wave plates and Δf is the unit distinction between each two frequencies.

Scrambling speed is a key factor for the improvement of the system performance. Optimal scrambling speed should be chosen to achieve moderate PMD tolerance. According to the recommendation in Ref. [5], the appropriate scrambling speed ranges from B/BECL to $B/(8\cdot d)$, where B is the bit rate, and d is the depth of interleaving. As Reed-Solomon (RS) encoder (255, 239) is used in our simulation and the interleaving depth is 16 symbols (i.e., 128 bits), the BECL equals 1,024 bits;

therefore, the fundamental frequency for the three wave plates of the FPS of Eq. (3) is at least 80 MHz. The unit distinction between each two frequencies is chosen as $\Delta f = 0.2$ MHz.

An 85-Gb/s optical system with DQPSK modulation is studied. Figure 1 illustrates the architecture of our simulation system. At the transmitter, useful redundant bits are added into the original information by a RS encoder (255, 239). Interleaving whose depth $d = 16$ (symbol), differential precoding, and conversion from one serial stream to two parallel branches are then operated before the electrical information is encoded into the optical phase shifts in both quadratures of the optical carrier. The receiver consists of a Guassian optical filter and the fifth-order Bessel electrical filters, whose 3-dB bandwidths are 72 and 26 GHz, respectively. Two Mach-Zehnder delay interferometers constitute the "self-homodyne" DQPSK receiver for demodulation of each quadrature, followed by balanced detection. The DQPSK signal can also be generated according to the method proposed in Ref. [11]. The received electrical information is processed by a symmetrical transformation of the RS decoder and deinterleaver.

In this mitigation scheme, the fiber link is divided into N sections by N distributed FPSs. For a given long optical link with a fixed PMD coefficient, because the length of the fiber sections between any two adjacent FPSs is not necessarily the same for different distribution patterns of FPS, the average DGD for each section is also different. Equation (1) is used to emulate the FPS.

In the simulation, the PMD emulator acts on the optical signal in the frequency domain, and its statistical model is detailed in Ref. [12], so it will introduce intersymbol interference. Meanwhile, FPS scrambles optical signal in the time domain as the commercial polarization scramblers are operated. On the other hand, the elements in the PMD vectors are discrete random variables, while the trace of the FPS scrambling is continuous on the Poincaré sphere.

To simulate the effect of the distributed FPS, five FPSs are distributed uniformly along the 500-km fiber link, of which the DGD/T (T is the period of a bit) of each section is 0.15. The pre-BER (BER: bit error rate) versus optical signal-noise ratio (OSNR) and the post-BER versus OSNR for systems with distributed FPS and without FPS are displayed in Fig. 2. When D-FPS is a part of the DQPSK system, the pre-BERs (crosses) are higher than those in the case where D-FPS is absent (lower triangles); meanwhile, the post-BER of the former (upper triangles) is lower than that of the latter (dots). The error correction capability of the FEC can be improved when it is combined with D-FPS. To further analyze the function of each frame after they propagate through the fiber link but before error correction in cases where D-FPS is present and absent, the OSNR equals 17 dB. We get 10^3 numbers, each of which indicates the number of error bits in each FEC frame for each case (i.e., the case with D-FPS and that without). The sum of the error bits in each certain range (the interval is 50) is divided base on the number of error bits in the FEC frame. Lastly, the ratios of the above sum to the total error bit of the 10^3 frames for both cases are computed.

Figure 3 illustrates the final error histogram, where Fig. 3(a) is the case where D-FPS is absent and Fig. 3(b) is the case where D-FPS is present. When the system does not contain the D-FPS, the sum of the ratio whose number of error bits is over 400 is about 33%. The similar sum of the ratio corresponding to the system with D-FPS is only about 6.3%. In the case of the former, it is considerable that the ratio of the related number of error bits is over 1,000, whereas the corresponding ratio in case of the latter is zero. Although the pre-BER is increased when the D-FPS is deployed along the optical link, it can avoid large numbers of error bits in the FEC frame. Because the short errors can be corrected effectively by FEC, the PMD tolerance of the system is increased.

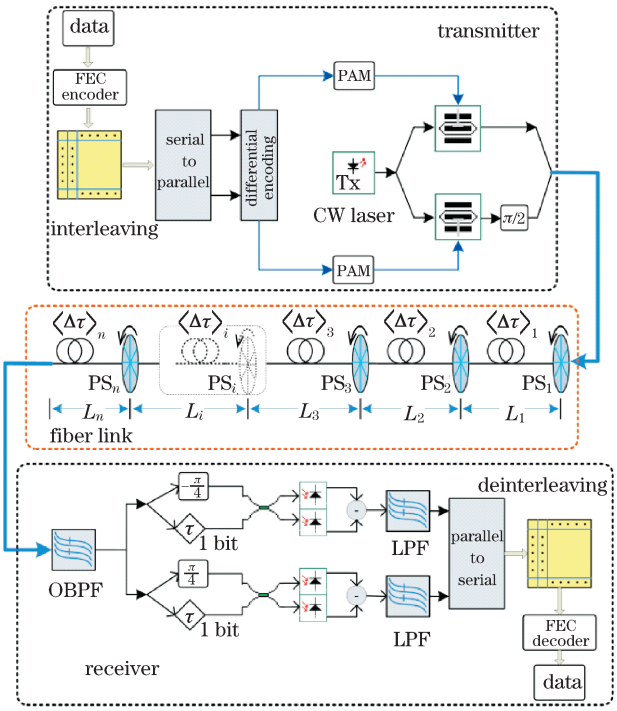

Fig. 1. System diagram of PMD mitigation with distributed FPS and FEC for DQPSK modulation. PAM: pulse-amplitude modulation; LPF: low-pass filter; OBPF: optical band-pass filter; Tx: transmit; PS: polarization scrambler.

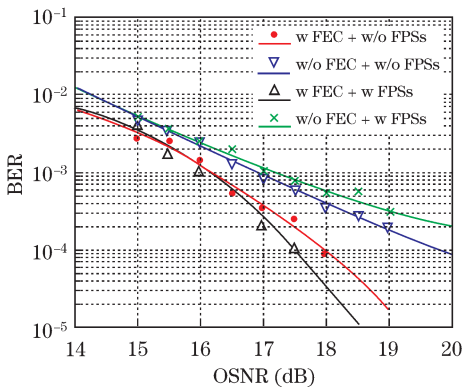

Fig. 2. BER versus OSNR for system without FPS in which pre-BER (lower triangles) and post-BER (solid circles) are measured, and system with FPS in which pre-BER (crosses) and post-BER (upper triangles) are measured. w: with; w/o: without.

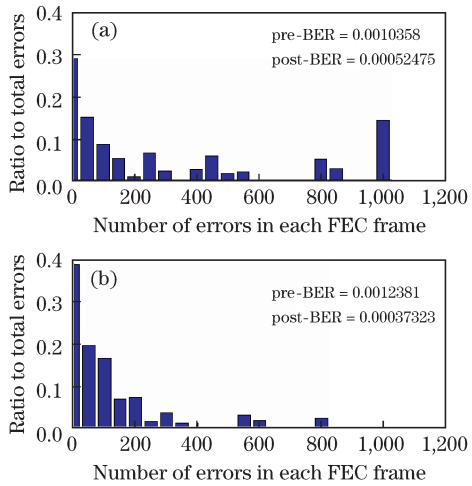

Fig. 3. Error histogram used to count the ratios of the number of errors in each FEC frames to the total errors (a) without FPS and (b) with FPS.

Table 1. Five Distribution Patterns of FPS (Unit: km)

	L_1	L_2	L_3	L_4
Model 1	125	125	125	125
Model 2	55	75	95	115
Model 3	195	175	155	135
Model 4	50	100	150	200
Model 5	200	150	100	50
	L_5	L_6	L_7	L_8
Model 1	125	125	125	125
Model 2	135	155	175	195
Model 3	115	95	75	55
Model 4	200	150	100	50
Model 5	50	100	150	200

Eight FPSs are distributed in a 1,000-km fiber link whose PMD coefficient $\tau' = 0.25$ ps·km$^{-\frac{1}{2}}$, and five distribution patterns of the FPSs are designed to investigate the effect for the different distribution patterns of D-FPS in the PMD mitigation scheme. Table 1 renders the length of each section divided by eight FPSs. The average DGD between two adjacent FPSs in a specific distributed pattern is

$$\langle \mathrm{DGD} \rangle_i = \sqrt{\tau'^2 \cdot L_i} = \sqrt{(0.25)^2 \cdot L_i}, \tag{4}$$

where $L_i\,(i = 1, 2, \cdots, 8)$ is the length of the fiber section. The total average DGD of the whole links can be calculated as shown in the following equation:

$$\langle \mathrm{DGD} \rangle = \sqrt{\langle \mathrm{DGD} \rangle_1^2 + \langle \mathrm{DGD} \rangle_2^2 + \cdots + \langle \mathrm{DGD} \rangle_8^2}. \tag{5}$$

As shown in Fig. 4, compared with the case where D-FPS is absent, the system with D-FPS shows a better performance, whatever distribution pattern of the D-FPS is used. The ability for performance improvement

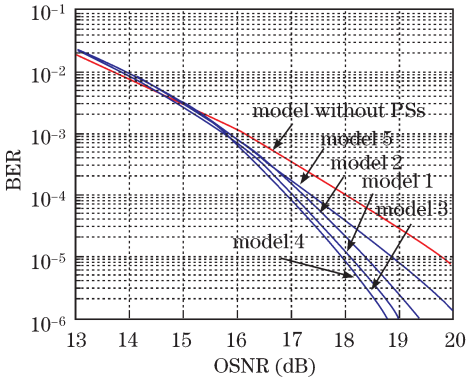

Fig. 4. BER versus OSNR for the system without FPS and the system with FPS.

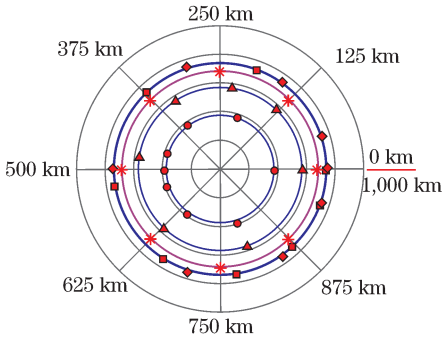

Fig. 5. Ring chart used to illustrate the performance of PMD mitigation for different distribution patterns of FPS where BER = 10^{-5}.

for different distribution patterns varies. The uniform distribution of the D-FPS, which is used in many previous studies, is not the optimal distribution style. Models 3 and 4 perform better than the uniform distribution. In the case where BER = 10^{-5}, compared with the uniform distribution, the requirement for OSNR of models 3 and 4 decreases by 0.134 and 0.167 dB, respectively.

The "ring chart" in Fig. 5 is a novel representation to assess the performance of different distribution patterns intuitively. We converse the length of each section into angle by the following equation:

$$\theta = \frac{L}{2\pi} \cdot L_i, \quad i = 1, 2, \cdots, 8, \tag{6}$$

where L is the total length of the fiber link and L_i is the length of each section that is divided by D-FPS. We then define the radius of each ring as the OSNR margin between a specific model and the case without D-FPS at a given BER (e.g., 10^{-5}). The performance is better when the radius is longer. The respective radius of models 3 (squares) and 4 (diamonds) are longer than those of the uniform distribution (stars), hence the two distribution patterns have better performance than the uniform distribution. In addition, the respective radius of models 2 and 5 are shorter than that of the uniform distribution, thus, their performances are worse than that of the uniform distribution.

However, in order to find the optimal distribution pattern of D-FPS for this PMD mitigation scheme, more

patterns should be included, and more simulations and experiments should be conducted. Other factors also have influence on the PMD mitigation with polarization scrambling and FEC in the DQPSK system. Because the RS coding and interleaving are performed in the level of symbols, the performance of the FEC will be reduced if the consecutive errors are dispersed overly through scrambling. Meanwhile, enhanced FEC can perform better than standard RS codes[13]. Future simulation and experiment to improve the performance of this PMD mitigation scheme are in progress.

In conclusion, the combination of FEC and D-FPS is necessary to expand the system's PMD tolerance. The function of the D-FPS in this scheme is to avoid large numbers of error bits in the FEC frame caused by PMD. The ability for performance improvement for different distribution patterns of D-FPS along the fiber link varies. The ring chart is developed to assess the performance of different distribution patterns intuitively.

This work was supported in part by the National "973" Program of China (No. 2010CB328204), the National "863" Project of China (No. 2009AA01Z224), the National Natural Science Foundation of China (Nos. 60772022 and 60932004), and the National "111" Project of China (No. B07005).

References

1. F. Tian, L. Xi, X. Zhang, X. Weng, G. Zhang, and Q. Xiong, Chin. Opt. Lett. **8,** 816 (2010).
2. H. Bülow, C. Xie, A. Klekamp, X. Liu, and B. Franz, Bell Labs Tech. Journal **14,** 105 (2009).
3. X. Liu, C. R. Giles, X. Wei, A. J. van Wijngaarden, Y.-H. Kao, C. Xie, and L. Möller, in *Proceedings of ECOC 2005* 343 (2005).
4. H. Bülow, in *Proceedings of ECOC 2006* Th.2.5.2 (2006).
5. X. Liu, C. Xie, and A. J. van Wijingaarden, IEEE Photon. Technol. Lett. **16,** 2183 (2004).
6. K. Ho and C. Lin, IEEE Photon. Technol. Lett. **9,** 1288 (1997).
7. C. Xie, X. Liu, and H. Bülow, IEEE Photon. Technol. Lett. **20,** 440 (2008).
8. X. Liu, in *Proceedings of OFC 2007* OMH4 (2007).
9. X. Zhang and Y. Zheng, Chin. Phys. B **17,** 1674 (2008).
10. J. P. Gordon and H. Kogelnik, PNAS **97,** 4541 (2000).
11. J. He, L. Chen, and S. Wen, Chin. Opt. Lett. **7,** 15 (2009).
12. A. Vannucci and A. Bononi, J. Lightwave Technol. **20,** 811 (2002).
13. A. Klekamp, D. Werner, and H. Bülow, in *Proceedings of OFC/NFOEC 2008* JWA54 (2008).